Pore-Scale Computational Study of Permeability and Pore Space Geometry in Gas Condensate Reservoir Rocks

V. V. Khimulia and V. I. Karev

Abstract This paper presents the results of quantitative and qualitative studies of pore space and filtration properties of rocks of gas condensate fields based on computed tomography images. The research was carried out using ProCon X-Ray CT-MINI high-resolution scanner of the Institute for Problems in Mechanics RAS. The approach for digitally analyzing CT images using the GeoDict package is described in detail. 3D structures of the studied rocks with separation of matrix and pore space were obtained on the basis of CT images. The main filtration-capacitance properties of the rock—porosity and permeability—were determined. The digitally obtained values are in good agreement with laboratory permeability measurements, which indicates the correctness of the applied approach. It is shown that the filtration properties of the rock are close to isotropic with weak transversal anisotropy. For detailed analysis of pore space and reasons of anisotropy appearance, geodesic tortuosity measurements and analysis of percolation paths were carried out. The local porosity point distribution along the directions in the specimen was obtained, and the connectivity of the pore space was evaluated. It is shown that the causes of permeability anisotropy are a combination of pore space features, such as different channel tortuosity along the directions in the rock, different width of percolation paths, local porosity variation along specimen slices, and non-uniform distribution of pore space connectivity. The data necessary for filling the hydrodynamic model of the field, as well as for a better understanding of the fundamentals of the relationship between the filtration process and the structure of the pore space in rocks were obtained. The conducted digital studies are an irreplaceable tool for studying the internal structure of rocks, as well as they complement and expand significantly the range of results obtained by laboratory methods. Their application in conjunction with classical rock testing can help solve important problems in the oil and gas production industry, such as permeability drop in the vicinity of wells, loss of wellbore stability, sand production and operational accidents.

V. V. Khimulia (✉) · V. I. Karev
Ishlinsky Institute for Problems in Mechanics RAS, Moscow, Russia
e-mail: valery.khim@gmail.com

V. Karev (ed.), *Proceedings of the 9th International Conference on Physical and Mathematical Modelling of Earth and Environmental Processes*, Springer Proceedings in Earth and Environmental Sciences, https://doi.org/10.1007/978-3-031-54589-4_26

Keywords Permeability anisotropy · Porosity · Reservoir filtration properties · Percolation paths · Geodesic tortuosity · Pore space structure · Computed tomography (CT) · GeoDict software · Gas reservoir properties

1 Introduction

The Arctic shelf is a huge treasure trove of hydrocarbons: oil and gas deposits already explored account for a quarter of the world's reserves. The northern shelf of Russia contains up to 25% of the country's oil reserves and up to 70% of its total explored gas reserves. However, the development of the Arctic region is currently facing significant challenges. These challenges primarily stem from the complexities associated with field development and operations in the demanding Arctic offshore conditions, and elevated economic costs. This difficulty is particularly prominent in the case of gas and gas condensate reservoirs found in the Russian Arctic shelf. These reservoirs are often weakly cemented, highly permeable sandstones with relatively low strength properties. Successfully developing and exploiting such reservoirs necessitates thorough and multifaceted preliminary investigations of core materials. These investigations are vital for creating adequate geomechanical and hydrodynamic models necessary for mitigating undesirable processes in wells, including sand production, loss of wellbore stability, and reductions in permeability in the bottomhole zones.

Comprehending the physical properties of reservoir rocks plays a pivotal role in the development of reservoir models and the innovation of strategies to enhance well productivity. To construct adequate hydrodynamic and geological reservoir models, extensive and thorough studies are essential, including laboratory core analysis. The primary reservoir characteristics that significantly impact reservoir processes include porosity, permeability, matrix structure, and rock pore space [1]. Traditionally, the assessment of rock permeability and porosity have been based on laboratory tests, well logging data, or indirectly through correlations with other rock characteristics [2]. There is a relatively recent and promising approach to studying rock properties in the laboratory—the numerical simulation of filtration processes using structures obtained through microcomputed X-ray tomography (μCT).

X-ray computed tomography (CT) represents a significant non-destructive technique for inspecting the internal structure of rocks, providing a valuable complement to direct laboratory investigations. This method entails reconstructing the spatial distribution of X-ray linear attenuation coefficients through computer processing of acquired projections during the radiation scan. The result of a CT examination is presented as a series of grayscale images collectively forming a three-dimensional depiction of X-ray absorption within the examined specimen [3]. Specialized software is subsequently employed to determine attributes such as linear dimensions, quantity, sphericity, and anisotropy of elements within the specimen [4]. To enable quantitative material analysis and the utilization of tomography results for numerical process modeling, image segmentation becomes imperative [5]. Segmentation is a technique involving the analysis of images and the transition from X-ray absorption to the spatial distribution of the specimen's constituent components within the specimen space. Segmentation can take the form of binary (two-phase) or multiphase segmentation. In the industry, pore imaging experiments combined with modeling serve as valuable tools for determining geological and physical properties [6], including porosity and permeability [7]. The calculations are conducted on a segmented image, primarily focusing on the macropore space. This space comprises pores with well-defined boundaries that can be effectively segmented into fluid and solid grains on a voxel basis [8].

Recent research combined with extensive experience in developing complex hydrocarbon fields has underscored the significant influence of reservoir property heterogeneity and anisotropy on mass transfer processes within reservoirs. Considering the anisotropy of filtration properties is crucial for addressing challenges in production optimization and enhancing recovery rates. Reservoir models that disregard permeability anisotropy often lead to either overestimation or underestimation of critical reservoir characteristics potentially causing substantial economic setbacks for the industry. Moreover, information about reservoir permeability anisotropy proves invaluable when determining the most suitable field development approach [9]. Furthermore, factors like bedding, layering, shear, and compaction can impede fluid flow [10]. It's widely acknowledged that various degrees of reservoir structure heterogeneity and filtration property distribution are present in most fields [11]. The permeability anisotropy within rocks significantly affects fluid flow within reservoirs, spanning from injection wells to production wells. This impact becomes particularly pronounced in the later stages of field development and can lead to a reduced reservoir coverage factor, especially for facilities equipped with horizontal wells [12].

One of the significant advantages of methods based on tomography data is the possibility of detailed analysis of pore space, including its connectivity, tortuosity of filtration paths, pore volume distribution, etc. Structural analysis of pore space allows quantitative assessment of the causes of anisotropy of filtration properties, which is a tremendous advantage compared to other methods of materials research.

This work presents the results of rock structure digital studies carried out on the base of ProCon X-Ray CT-MINI high-resolution scanner of the Institute for Problems in Mechanics RAS. 3D structures of rocks under study were created on the basis of tomography images. Numerical and quantitative analysis of pore distribution in the rock was carried out, pore space connectivity and pore distribution in rock slices were investigated. Images of percolation paths were obtained and the tortuosity of filtration paths in the rock was estimated. Numerical modeling of the filtration process was carried out, permeability values of rocks in three directions were obtained. The data necessary for filling the hydrodynamic model of the field, as well as for a better understanding of the relationship between the filtration process and the structure of the pore space in rocks were obtained. It is shown that the data obtained by modeling on high-resolution images correlate closely with laboratory measured permeability values.

2 Research Methodology

The core material under investigation was obtained from a gas condensate field located on the Arctic shelf of Russia. The rocks under study were sandstone, which has high porosity and low strength. A series of high-resolution tomographic images were taken to obtain a clear picture of the internal structure. Specimens were randomly shaped pieces of the core with dimensions of 5–20 mm to get maximize resolution. The orientation of the axes in the specimens corresponded to the rock layering axes.

The procedure for computed tomography and image acquisition of the specimens was carried out using the ProCon X-Ray CT-MINI high-resolution micro-CT scanner of the Institute for Problems in Mechanics RAS [13]. This device boasts dimensions of $1300 \times 850 \times 600$ mm and incorporates a robust base constructed from a single monolithic granite slab. This design choice effectively eliminates temperature-induced drift and ensures precise alignment of X-ray optical components and other system elements within the device, guaranteeing measurement accuracy and stability across the entire operational range.

The scanner employs a vertical core placement scheme for research purposes, accommodating specimens with a maximum height of 200 mm and a maximum diameter of 200 mm. The device is capable of handling loaded specimens weighing up to 5 kg. To enable precise measurements, a precision positioning system (manipulator) is integrated into the design allowing for a distance of 335 mm from the tube to the object. Furthermore, the detector can move perpendicular to the main system axis within a range of ± 25 mm. The manipulator enables a 360-degree rotation of the specimen around its axis, achieving angular position reproducibility accuracy of 1.5 angular seconds. The microfocus X-ray tube, known for its high resolution and closed-loop operation, offers an adjustable output voltage range from 20 to 90 kV and an adjustable current range from 10 μA to 160 μA. The tube's maximum output power reaches 8 W, with the smallest focal spot size measuring 5 μm. The X-ray detector characterized by high sensitivity and minimal noise features a pixel count of 2940×2304 and a pixel size of 49.5 μm. The active (sensitive) area of the detector spans 146×114 mm.

The scans were reconstructed using VGSTUDIO software, while 3D image processing was carried out using Geodict Math2Market GmbH software [14]. GeoDict is an all-encompassing platform designed for multifaceted 3D image processing, material modeling, visualization, material property assessment, material development via modeling, and process optimization. Beyond its core image processing functionalities, GeoDict offers a range of techniques for image segmentation. Furthermore, GeoDict provides a wide array of solution methods for modeling fluid flow, conductivity, and mechanical behavior within porous media, accommodating both single-phase and two-phase scenarios.

Filtration fields were determined using the FlowDict module from the GeoDict package [15]. This module predicts effective material properties, including flow velocity, flow permeability, and flow resistivity, by simulating flow experiments and subsequently analyzing the simulation results. FlowDict predicts the mean flow velocity under specific pressure conditions [16] and calculates the permeability of a porous structure by applying Darcy's law. This versatile module is proficient in computing incompressible, stationary Newtonian flows, employing various approximations derived from the Navier–Stokes equations. FlowDict is widely utilized by researchers worldwide for modeling flows in a variety of materials [17–20]. In this study, LIR solver was employed for numerical filtration simulations [21]. LIR is distinguished as the most recent and remarkably fast iterative finite volume method. This solver computes not only permeability but also velocity and pressure fields within extensive three-dimensional images. The convergence rate depends on the complexity and heterogeneity of the pore space. The chosen termination criterion for the flow simulations is the error bound, which possesses the capability to detect convergence oscillations and prevent premature termination of the process at local minima or maxima [22]. Specifically, the termination threshold was established at 0.1 for the LIR solver, causing it to halt once the relative difference in comparison to the prediction becomes less than 0.1. Additionally, Multigrid was utilized in the calculations, a technique that revolves around employing multiple coarser adaptive grids to expedite convergence while requiring minimal additional memory [23].

To evaluate the geometric and statistical homogeneity of the pore space across all specimens, porometric analysis and visualized pore geometry using MatDict [24] and the PoroDict modules were conducted, both of which are based on segmented images.

3 Experimental and Simulation Results

High-resolution computed tomography images were taken of all five specimens. These images offer clear differentiation between grain and pore boundaries, enabling statistical quantitative analysis and modeling. All high-resolution imaging was conducted with the following parameters: a source voltage of 90 kV, an amperage of 89 μA, an exposure time of 0.2 s, 15 averages for each projection, a rotation step of 0.125 degrees, and a voxel size of 4.957 μm. Following scanning and reconstruction, in-depth image processing was carried out using GeoDict software.

To enhance image quality and streamline the segmentation process, the Non-Local Means (NLM) filter was applied. Figure 1a displays the high-resolution projection obtained after reconstruction. For segmentation purposes, the Global Thresholding method was employed to refine the grain boundaries, as illustrated in Fig. 1b.

Further digital research was carried out on the basis of the established structures. A porosity-based representative elementary volume (REV) analysis was performed. It showed that for these rocks, a representative volume starts with a linear cubic structure size of more than 200 voxels. The structures used for the analysis had linear sizes of 500 voxels. Open porosity was estimated for all specimens using PoroDict module. On average, the porosity of the described series of specimens varied between 29 and 34%. Further results of the study will be presented using a typical specimen with

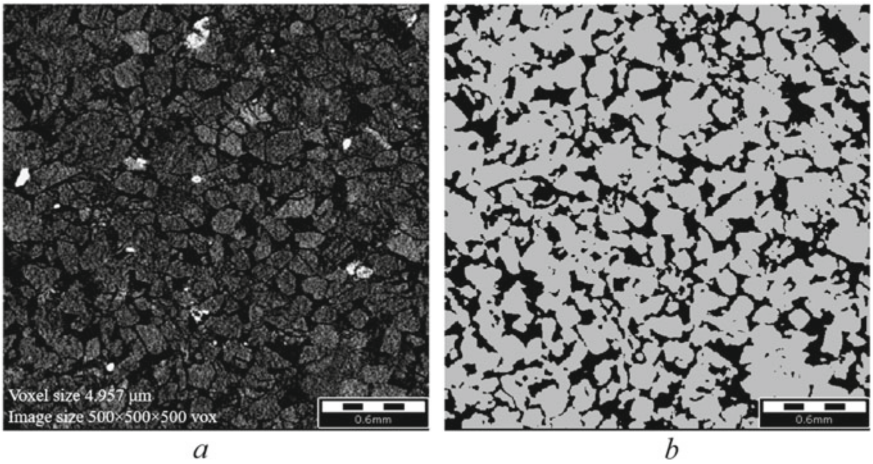

Fig. 1. **a**—slice of high-resolution 3D image after reconstruction; **b**—same slice after segmentation (grey—matrix material, black—pores)

porosity of 33.9%. Figure 2a shows the full 3D structure of the described specimen after processing and segmentation. Figure 2b shows the rock matrix obtained after segmentation. Figure 2c shows the pore space structure of the specimen.

Laboratory measurements of rock permeability were performed to determine the filtration properties of the specimen and to compare with the results obtained by digital method. For all specimens, permeability measurements were conducted using the TILTS facility of the Institute for Problems in Mechanics RAS [25]. For this purpose, cubic specimens with 40 mm edge were made from core material. During permeability measurement specimens were covered with an impermeable film along four edges parallel to the permeability measurement axis. Then air was

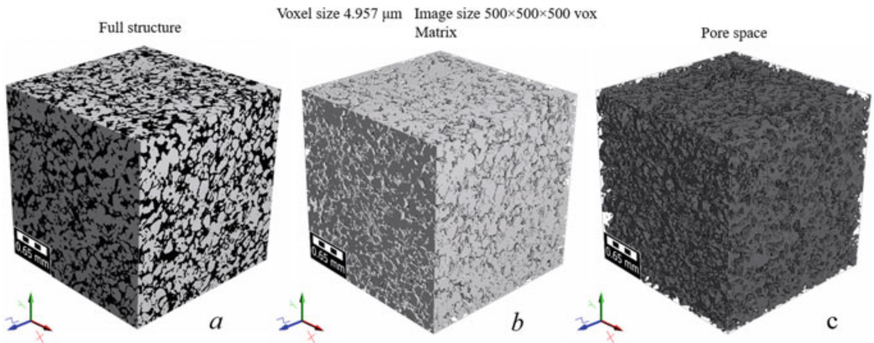

Fig. 2 **a**—full 3D structure of the described specimen after processing and segmentation (grey—matrix material, black—pores); **b**—rock matrix obtained after segmentation; c—pore space structure of the specimen

passed through two open faces under a small pressure drop (0.01 MPa) and its flow rate was measured [26]. The results of permeability measurements along and across the bedding for the tested rock are presented in Table 1, column 3. As it can be seen from the table, the rock has high permeability. It differs insignificantly in the directions along and across the bedding, which indicates a weak degree of transversal anisotropy of the rock in terms of filtration properties.

To evaluate the filtration properties and their anisotropy, a filtration flow modeling procedure was conducted. To simulate the filtration flow within the resulting structure, the Navier–Stokes filtration model was employed using the FlowDict module [15]. To simulate the conditions of laboratory permeability measurements, the following flow parameters were set: fluid is air, a pressure drop of 0.01 MPa, a temperature of 20 s°C, and boundary conditions in the filtration direction set to periodic with an implicit region of 10 voxels (inlet and outlet regions before and after the computed region to homogenize the flow. Additionally, in the tangential direction of structure, symmetric boundary conditions were applied. The results of the simulation on the example of the described specimen are presented in Table 1, column 4. As evidently from the table, the computed permeability closely aligns with the laboratory data. Furthermore, the permeability along the core axis consistently remains lower than in the layering directions. The difference between the values obtained by laboratory and numerical method is not more than 5%, which is a very good result for numerical modeling and confirms the correctness of the chosen model and the created methodology.

The pore space was digitally analyzed using MatDict and PoroDict for a more detailed study of the pore space and the causes of anisotropy.

Geodesic tortuosity values were measured for each direction in the specimen. The mean geodesic tortuosity quantifies the length of paths through the transport phase [27]. To compute it from 3D image data, all shortest paths beginning at the inflow plane were calculated. Tortuosity is defined as the average over all shortest path lengths divided by the thickness of the material [28]. The results of this analysis are presented in column 5 of Table 1. Comparison of the results on three axes shows that the values differ insignificantly. This is evidence of high connectivity of the

Table 1 Results of measurements and digital analysis

Direction in rock	Specimen axis	Laboratory value of permeability, D	Calculated permeability, D	Mean geodesic tortuosity	Minimal pore volume fraction	Mean number of connected pores in direction
Across the bedding (X)	X	5.200	5.455	1.05922	0.088	1060.26
Along the bedding (Y–Z)	Y	5.500	5.820	1.05640	0.118	1075.78
	Z		5.516	1.05651	0.110	1077.24

pore space on all axes. It can be seen that the value of tortuosity perpendicular to the bedding plane has a higher value. As a consequence, the permeability along this direction is lower than in other directions. At the same time, the tortuosity in both directions along the bedding differs insignificantly, despite the difference in permeability values. However, the trend of correlation remains: higher tortuosity corresponds to lower permeability. Thus, it is confirmed that tortuosity can be used in comparative assessment of rock filtration properties. The accuracy of this assessment will depend on the range of permeability values being compared. At the same time, the tortuosity parameter takes into account only the length of the filtration path in the direction, but does not take into account the width and size of particles able to pass along this path. Therefore, hydrodynamic models based only on this parameter may not reflect the actual values of permeability.

The PoroDict module was applied to estimate characteristic pore sizes. The results of the analysis showed that the pore space includes pores with sizes ranging from 10 μm to 140 μm. The highest number of pores have sizes of 20–30 μm and 35–45 μm. At the same time, pores larger than 50 μm account for 30% or more of the total volume. However, despite the large pore widths, filtration fluxes are known to be estimated by the smallest pore size through which a particle must pass during movement. To study them, calculations of percolation pathways were performed. To compute percolation paths, the MatDict method identifies the maximum diameters of spherical particles capable of traversing through the medium. Moreover, it calculates and presents the shortest paths taken by the largest particles. A visualization of 100 random percolation paths is presented in Fig. 3 for two directions in the rock: perpendicular to the bedding (X-axis, Fig. 3a) and along the bedding (Y-axis, Fig. 3b).

For each path, the maximum diameter of a particle capable of traveling along is calculated. In the direction perpendicular to the bedding, the maximum path widths ranged from 18 to 28 μm. In the direction along the bedding, the paths were slightly wider: from 20 to 30.5 μm. Such insignificant differences in the sizes of particles able to pass along the calculated paths define to the differences of permeability values

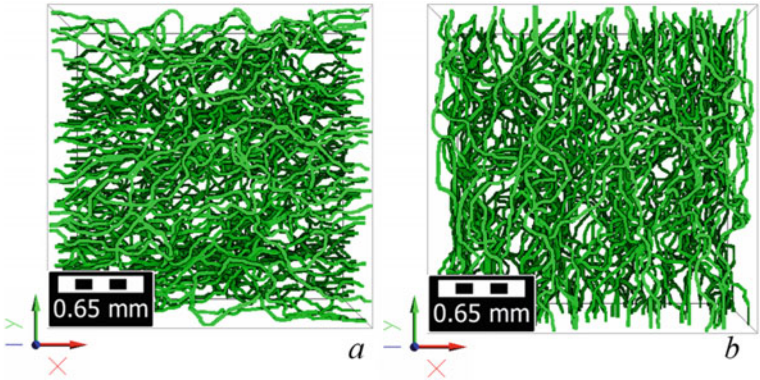

Fig. 3 **a**—Percolation paths perpendicular to bedding; **b**—percolation paths along the bedding

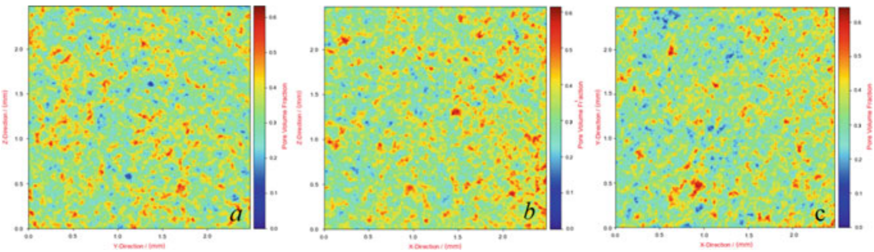

Fig. 4 Distribution of pore volume fraction along the X-direction (**a**), Y-direction (**b**) and Z-direction (**c**)

along different directions and confirm the weak degree of permeability anisotropy. For the structure with a linear size of 2.479 mm (500 voxels), the average percolation path lengths for the X and Y axes were 4.424 and 4.474 mm, respectively. Thus, the path lengths differ slightly along the axes (by 1.1%), with the calculated paths being slightly shorter along the X axis.

To integrally evaluate the pore distribution along each axis of the specimen, 2D Density maps were made. Such distributions are created based on the calculation of the distribution of Pore Volume Fraction in a plane normal to the chosen direction. Each pixel of the plots is calculated by averaging the respective porosity in the direction of interest. Figure 4 shows the integral porosity distributions along each axis of the specimen. The axes of each graph show the specimen lengths in mm along the directions perpendicular to the one under consideration. The color indicates the average porosity values of all pixels along the selected specimen direction.

As it can be seen from these maps, the porosity distribution along each direction is generally uniform. The low porosity (blue) and high porosity (red) regions are homogeneously distributed. On average, the porosity distribution along each axis corresponds to an overall bulk porosity value of 0.33. That is, the filtration process along each axis takes place throughout the entire volume of the specimen, without the strong dominance of isolated highly permeable paths. Meanwhile, it can be seen from Fig. 4b that along the Y direction of the specimen, the highest porosity is slightly concentrated in the right part of the specimen (end of the X axis). This may be the reason for the increased permeability along this direction. Moreover, this occurrence was not seen when analyzing the percolation paths due to their randomness of calculation. The minimum values of pore volume fraction (porosity) in each direction are presented in column 6 of Table 1. Described method allows to evaluate the contribution of porosity to the distribution of filtration fluxes in the presence of a pore space connectedness. However, for an accurate conclusion about the contribution of the local porosity distribution to the filtration properties of the rock, it is necessary to evaluate the connectivity of the pore space in each direction. Even for highly porous rocks, the permeability may differ significantly depending on the number of pore connections.

To analyze the connectivity of the pore space, the Identify Pores methods along with Connected Components of the GeoDict package were applied. The Identify

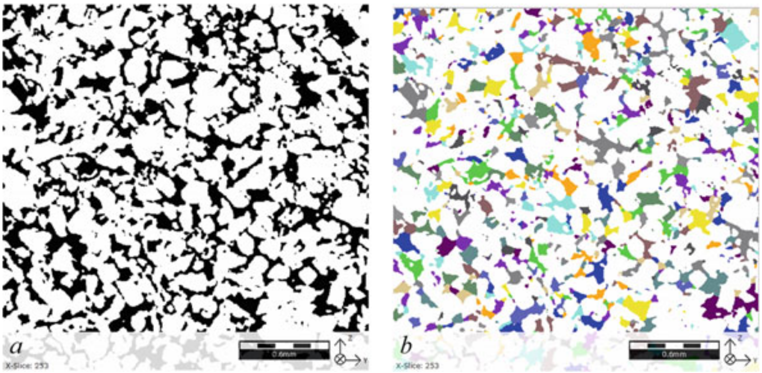

Fig. 5 **a**—slice of the described 3D specimen structure (white is rock matrix, black are pores); the same slice after pore space separation into pores (color shows different pores, white is rock matrix)

Pores method allows, based on additional segmentation, to identify individual pores in the pore space, estimate their size, volume and contact surfaces. The Connected Components method analyzes the voxel-to-voxel relations of the pores or solid material and computes the components that build up the pore fraction. Through this method it is possible to find and count the number of connected components in the 3D structure. A connected component consists of all voxels that are in contact with each other, and which belong to the same phase. Results of the method include the mean number of components per 2D slice in each spatial direction.

Figure 5 shows the result of pore space separation into individual pores. On the left picture is presented a slice of the described structure before the algorithm was applied, on the right one is presented the result of pore separation.

The newly obtained structure was used to apply the Connected Components method, which resulted the distributions of connected pores along each direction in the specimen. Figure 6 shows plots of the number of connected pores for each slice of the structure along the three selected directions.

The plots show that the number of connected components in layers along the bedding axes (Y, Z) is almost identical. The number of connected pores is distributed almost uniformly along planes in three directions with a small deviation from the average value. For the X axis, a more pronounced increase in the number of bound pores is observed along the growth of the layer number. This is due to the previously indicated compaction of the high porosity distribution in the growth region of the X-axis seen in Fig. 4b and the discreet localization of low porosity at the beginning of the X-axis (Fig. 4c). These plots demonstrate well the relationship of the quantitative porosity distribution with the connectivity of the pore space. In this case, the most understandable value when analyzing the influence of this parameter on the filtration properties of the rock will be the average value of connected pores along the selected direction. Table 1, column 7 shows the average values of the number of connected components for each axis of the specimen. It can be observed that the direction perpendicular to the bedding (X) corresponds to a lower value of average connectivity,

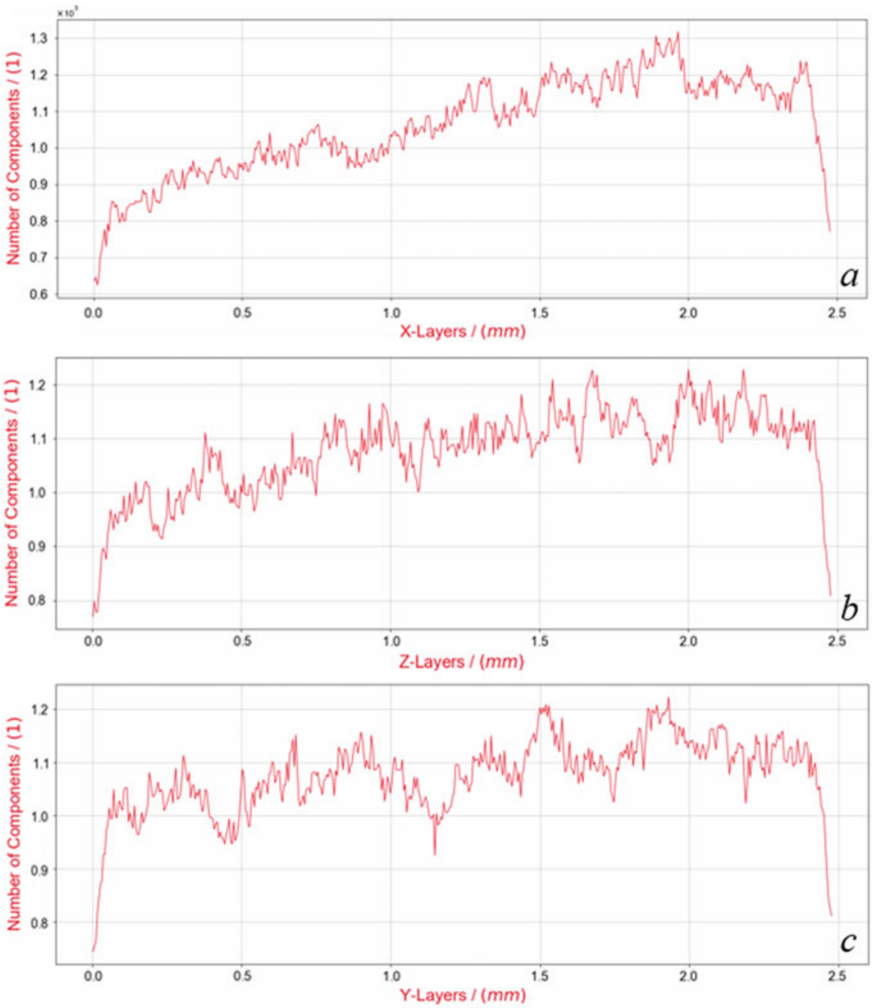

Fig. 6 Number of connected pores for each layer along the X direction (**a**), Z-direction (**b**) and Y-direction (**c**)

while for the Y and Z axes the values are higher and almost equal to each other. This is also a quantitative assessment of the cause of permeability anisotropy in the rock.

The data acquired in this study represent the initial phase of our planned comprehensive examination of the rocks in this deposit. These rocks of the studied interval have a weak degree of transversal isotropy and are practically isotropic in filtration properties. The anisotropy is caused by a local increase in average porosity and pore connectivity along the bedding direction, as well as by the resulting decrease in channel tortuosity and a slight increase in channel width in this direction. The results obtained through numerical analysis demonstrate well agreement with traditional laboratory tests conducted on similar rocks from Arctic gas fields [29].

The studies described can be extended and refined by additional quantitative evaluation of the material: grain and pore sorting, roundness, packing characteristics and mineral composition. The digital analysis applied to CT images, as demonstrated in this study, proves to be a valuable addition to both laboratory-based and in-situ investigations of reservoir properties.

4 Conclusion

Thus the paper presents the results of digital studies conducted on the pore space and filtration properties of Arctic gas condensate field reservoir rocks. These studies are based on computed tomography (CT) images obtained using the ProCon X-Ray CT-MINI high-resolution scanner of the Institute for Problems in Mechanics RAS. The paper provides a detailed description of the methodology used to digitally analyze CT images using the GeoDict package. Through this analysis, 3D structures of the rocks under investigation were created with a clear separation between the matrix and pore space based on the CT images. The primary filtration-related properties of the rock, namely porosity and permeability, were determined. The digitally obtained values are close to the results of laboratory permeability measurements confirming the accuracy of the applied approach. The study reveals that the filtration properties of the rock are nearly isotropic, there is only weak transverse anisotropy. To delve deeper into the analysis of the pore space and understand the reasons for the observed anisotropy, the study also conducted geodesic tortuosity measurements and analyzed percolation paths. It included evaluating the local distribution of porosity within the specimen and assessing the connectivity of the pore space. The study concludes that the causes of permeability anisotropy are a combination of pore space characteristics, such as varying channel tortuosity along different directions within the rock, differences in percolation path widths, local porosity fluctuations across specimen slices, and non-uniform distribution of pore space connectivity.

The data obtained from this study are essential for developing the hydrodynamic model of the gas field. They also provide a deeper understanding of the relationship between the filtration process and the structure of pore space in rocks. The digital investigations conducted in this study are an important tool for examining the internal structure of rocks and significantly complement and expand the range of results obtained through traditional laboratory methods. The combined application of these digital techniques with classical rock testing can help address critical challenges in the gas production industry, including issues like permeability reduction near wells, wellbore stability problems, sand production, and other operational incidents.

Acknowledgements The Research Was Supported by the Russian Science Foundation Grant № 23–77-01,037, https://rscf.ru/project/23-77-01037/

References

1. Ganat T. A. A. O. Fundamentals of reservoir rock properties. – Cham, Switzerland: Springer, 2020. https://doi.org/10.1007/978-3-030-28140-3.
2. Ivanov M.K. et al. Petrophysical Methods for Study of Core Material // M.: Publishing house of Moscow State University. 2008. P. 112. (in Russian).
3. Lichun J., Mian C. 3D imaging of fractures in carbonate rocks using X-ray computed tomography technology // Carbonates and Evaporites. 2014. V. 29. I. 2. pp. 147–153. https://doi.org/10.1007/s13146-013-0179-9
4. Diaz M. et al. Surface roughness characterization of open and closed rock joints in deep cores using X-ray computed tomography // International Journal of Rock Mechanics and Mining Sciences. 2017. V. 98. pp. 10-19. https://doi.org/10.1016/j.ijrmms.2017.07.001
5. Gerke K.M., Korost D.V., Karsanina M.V., Korost S.R., Vasiliev R.V., Lavrukhin E.V., Gafurova D.R. Modern approaches to pore space scale digital modeling of core structure and multiphase flow // Georesources. 2021. 23(2). pp. 197–213. https://doi.org/10.18599/grs.2021.2.20
6. Menke H.P. et al. Using Nano-XRM and High-Contrast Imaging to Inform Micro-Porosity Permeability During Stokes–Brinkman Single and Two-Phase Flow Simulations on Micro-CT Images // Frontiers in Water. 2022. V. 4. P. 935035. doi: https://doi.org/10.3389/frwa.2022.935035.
7. Blunt M.J. Multiphase Flow in Permeable Media: A Pore-scale Perspective // Cambridge: Cambridge University Press. 2017. doi: https://doi.org/10.1017/9781316145098
8. Mostaghimi P., Blunt M.J., Bijeljic B. Computations of absolute permeability on micro-CT images // Math. Geosci. 2013. V. 45. pp. 103–125. doi: https://doi.org/10.1007/s11004-012-9431-4
9. Krivoshchekov S., Kochnev A., Kozyrev N., Ozhgibesov E. Factoring Permeability Anisotropy in Complex Carbonate Reservoirs in Selecting an Optimum Field Development Strategy // Energies. 2022. 15 (23). 8866. https://doi.org/10.3390/en15238866
10. Vajdova V., Baud P., Wong T. Permeability evolution during localized deformation in Bentheim sandstone // J. Geophys. Res. 2004. 109. B10406, https://doi.org/10.1029/2003JB002942
11. Aliev Z.S., Kotlyarova E.M. Approximate method of UGS creation and operation in heterogeneous formations using horizontal wells. Envir. Responsib. of Oil and Gas Ind. 2017. 46–55 (in Russian).
12. Maksimov V.M., Dmitriev N.M., Antonievich Yu.S. Effects of tensor nature of relative phase permeabilities at mutual gas displacement by water in anisotropic reservoirs // Georesour., Geoenerg., Geopolit. 2010. 1 (1), 25 (in Russian).
13. CT-MINI by ProCon X-Ray GmbH available at https://procon-x-ray.de/en/ct-mini.
14. GeoDict – The Digital Material Laboratory: [digital source] URL: https://www.math2market.de/ (Date of request: 23.09.2023).
15. Hilden J., Cheng L., Linden S., Planas B. FlowDict User Guide GeoDict release 2022. Published: November 9, 2021. https://doi.org/10.30423/userguide.geodict2022-flowdict.
16. Kling T. et al. Simulating stress-dependent fluid flow in a fractured core sample using real-time X-ray CT data // Solid Earth. 2016. V. 7. 1109–1124. https://doi.org/10.5194/se-7-1109-2016
17. Herdtle T., Xue Y., Bolton J. S. Numerical modelling of the acoustics of low density fibrous media having a distribution of fiber sizes. Publications of the Ray W. Herrick Laboratories. 2017. Paper 167.
18. Balucan R. et al. Coal permeability stimulation by NaClO oxidation // The APPEA Journal. 2019. V. 59. №. 2. P. 846-850. https://doi.org/10.1071/AJ18142
19. Soltani P. et al. Experimental and computational analysis of sound absorption behavior in needled nonwovens // Journal of Sound and Vibration. 2018. V. 426. P. 1-18. https://doi.org/10.1016/j.jsv.2018.04.007
20. Steel K.M. et al. Identification of preferential pathways in the pore microstructure of metallurgical coke and links to anisotropic strength properties // Fuel. 2021. V. 296. P. 120688. https://doi.org/10.1016/j.fuel.2021.120688

21. Linden S. et al. The LIR space partitioning system applied to the Stokes equations // Graphical Models. 2015. V. 82. pp. 58-66. https://doi.org/10.1016/j.gmod.2015.06.003
22. Pan Z., Liang Y., Tang M. et al. Simulation of performance of fibrous filter media composed of cellulose and synthetic fibers // Cellulose. 2016. 26, 7051–7065. https://doi.org/10.1007/s10570-019-02605-8
23. Saxena et al. References and benchmarks for pore-scale flow simulated using micro-CT images of porous media and digital rocks // Advances in Water Resources. 2017. 109. pp. 211-235. https://doi.org/10.1016/j.advwatres.2017.09.007
24. Rief S., Hilden J., Planas B. MATDICT User Guide. GeoDict release 2022. December 8, 2021. https://doi.org/10.30423/userguide.geodict2022-matdict
25. Karev V., Kovalenko Y., Ustinov K. Advances in Oil and Gas Exploration and Production. Switzerland: Springer International Publishing. 2020. 166 p. https://doi.org/10.1007/978-3-030-26608-0
26. Karev V., Kovalenko Y. Triaxial loading system as a tool for solving geotechnical problems of oil and gas production. True triaxial testing of rocks. 2013. Leiden: CRC Press/Balkema: 301–310.
27. Holzer L., Marmet P., Fingerle M., Wiegmann A., Neumann M., & Schmidt V. Tortuosity and microstructure effects in porous media: classical theories, empirical data and modern methods. Springer Series in Materials Science. 2023. https://doi.org/10.1007/978-3-031-30477-4
28. Stenzel O., Pecho O., Holzer L., Neumann M., & Schmidt V. Predicting effective conductivities based on geometric microstructure characteristics // AIChE Journal. 2016. 62(5). pp. 1834-1843. https://doi.org/10.1002/aic.15160
29. Pyatakhin M. V., Shulepin S. A., & Gaidash Y. M. Experimental studies of reservoir rock fracture in the bottomhole zone of wells. Territory Neftegaz, 2020. (9-10), 30-37. (in Russian)